Title
Elastic membrane enabled inward pumping for liquid manipulation on a centrifugal microfluidic platform

Journal
Biomicrofluidics, 16(3)

ISSN
1932-1058

Authors
Liu, Yujia
Kulinsky, Lawrence
Shiri, Roya
et al.

Publication Date
2022-05-01

DOI
10.1063/5.0089112

Peer reviewed

Biomicrofluidics ARTICLE scitation.org/journal/bmf

Elastic membrane enabled inward pumping for liquid manipulation on a centrifugal microfluidic platform

Cite as: Biomicrofluidics 16, 034105 (2022); doi: 10.1063/5.0089112
Submitted: 22 February 2022 · Accepted: 20 April 2022 ·
Published Online: 18 May 2022

Yujia Liu,[1,a)] Lawrence Kulinsky,[2] Roya Shiri,[3] and Marc Madou[2,4,5,a)]

AFFILIATIONS

[1]Department of Materials Science and Engineering, University of California, Irvine, California 92707, USA
[2]Department of Mechanical and Aerospace Engineering, University of California, Irvine, California 92697, USA
[3]Autonomous Medical Devices Inc., Inglewood, California 90304, USA
[4]Department of Biomedical Engineering, University of California, Irvine, California 92697, USA
[5]Department of Chemical and Biomolecular Engineering, University of California, Irvine, California 92697, USA

[a)]**Authors to whom correspondence should be addressed:** yujial3@uci.edu and mmadou@uci.edu

ABSTRACT

Nowadays, centrifugal microfluidic platforms are finding wider acceptance for implementing point-of-care assays due to the simplicity of the controls, the versatility of the fluidic operations, and the ability to create a self-enclosed system, thus minimizing the risk of contamination for either the sample or surroundings. Despite these advantages, one of the inherent weaknesses of CD microfluidics is that all the sequential fluidic chambers and channels must be positioned radially since the centrifugal force acts from the center of the disk outward. Implementation of schemes where the liquid can be rerouted from the disk periphery to the disk center would significantly increase the utility of CD platforms and increase the rational utilization of the real estate on the disk. The present study outlines a novel utilization of elastic membranes covering fluidic chambers to implement inward pumping whereby the fluid is returned from the disk periphery to the center of the disk. When the disk revolves at an angular velocity of 3600 rpm, liquid enters the chamber covered by the elastic membrane. This membrane is deflected upward by liquid, storing energy like a compressed spring. When the angular velocity of the disk is reduced to 180 rpm and thus the centrifugal force is diminished, the elastic membrane pushes the liquid from the chamber inward, closer to the center of the disk. There are two channels leading from the elastic membrane-covered reservoir—one channel has a higher fluidic resistance and the other (wider) has a lower fluidic resistance. The geometry of these two channels determines the fluidic path inward (toward the center of the disk). Most of the liquid travels through the recirculating channel with lower resistance. We demonstrated an inward pumping efficiency in the range of 78%–89%. Elastic membrane-driven inward pumping was demonstrated for the application of enhanced fluid mixing. Additionally, to demonstrate the utility of the proposed pumping mechanism for multi-step assays on the disk, we implemented and tested a disk design that combines plasma separation and inward pumping.

I. INTRODUCTION

Centrifugal microfluidic platforms have been extensively investigated for potential application as a micro-total analysis system (μTAS), automating "sample-in-answer-out" biological assays, especially in point-of-care (POC) scenarios. Through different geometric chamber and channel designs and spin protocols, various fluidic manipulations such as sedimentation, mixing, valving, and metering[1–3] have been realized as the functional building blocks of many types of biological assays. To date, numerous biological assays such as polymerase chain reaction (PCR) assays, loop-mediated isothermal amplification (LAMP) assays, lateral flow assays, and microarray assays have been successfully demonstrated on the centrifugal microfluidic platform.[4–8]

Liquid on the compact disk (CD) is driven by three major inherent forces: centrifugal, Euler, and Coriolis. By nature, these forces either point radially outward (centrifugal force) or are

tangential to the circumference (Euler force and Coriolis force). Consequently, the net force acting on the liquid on a CD drives the liquid to flow from the center to the periphery of the disk (radially outward).[9] Therefore, a CD is usually designed in a way that the assay steps are performed sequentially outward. However, functional units, such as cell lysis, DNA extraction, blood/plasma separation, and reagent hybridization, which consist of multiple fluidic manipulation steps, take up a large portion of radial space on a CD.[10,11] As the assay becomes more complicated, the CD needs to be larger to accommodate the extra steps, but space remains unused due to one-directional radially outward flow of the fluid. A larger CD also imposes stricter requirements for the motor/power system. These obstacles restrict the degree of complexity of the assays that can be implemented on the CD platform. Therefore, a mechanism that pumps the liquid inward after the liquid reaches the edge of the CD is highly desirable. By enabling the fluid flow to proceed from the center outward and then be returned to the center, complex biological assays can be realized on the CD platform without increasing the size of the system, which is preferable for μTAS systems in POC applications.

Several types of inward pumping mechanisms have been developed that can be categorized as either active-pumping (also assisted pumping) or passive-pumping, depending on the presence or absence of external energy sources.[12,13] Active or assisted-pumping mechanisms use external components to apply thermal, mechanical, or electrical energy that drives the liquid on the disk inward. For example, Abi-Samra *et al.* developed a thermal-pneumatic pumping mechanism where the air in a ventless chamber expands under heating to pump liquid back to the center during spinning.[14] Another assisted pneumatic pumping mechanism was developed by Kong *et al.*, providing an inward pumping force by applying externally pressurized air through an opening on the CD.[15] In 2015, a mechanical inward pumping mechanism was achieved using a fly ball system, which acts on a chamber with a deformable polymer membrane in a direction perpendicular to the rotation plane, pushing the liquid in the same chamber inward during spinning.[16] With the introduction of electricity on a CD through either inductive coils or slip-rings, various electrical pumping mechanisms have been developed.[12,17] Electrolysis generating gas inside a ventless chamber can pump liquid inward with a similar disk configuration as in thermal-pneumatic pumping.[17,18] Direct pumping liquid back to the center has also been achieved by mounting electronic pumps directly on the disk.[12,19]

The passive-pumping mechanism, as its name implies, does not require external components to provide energy for pumping the liquid back to the disk center. Various disk configurations and spinning protocols have been demonstrated to achieve inward pumping. One of the simplest mechanisms relies on capillary force to bring liquid back to the center of the CD by using hydrophilic materials, allowing a portion of the liquid to flow back to its original chamber.[20] Pishbin *et al.* developed a mechanism that uses the Euler force generated by abrupt deceleration of the spinning disk from 2500 to 50 rpm. This way, liquid can be pumped to a chamber closer to the center of the disk through a guiding channel.[21] However, the requirement of surface treatment and a strong motor, as well as the low pumping efficiency, limit the implementation of this method in a practical assay. To achieve comparably higher pumping efficiencies, displacement pumping mechanisms were developed by using displacer liquids to pump target liquid inward.[22,23] Despite the higher efficiency, the sophisticated displacement mechanism requires too precise coordination among chambers and preloaded liquids. Another high-efficiency pumping mechanism, dynamic-pneumatic pumping based on compressing air in a ventless rigid chamber, was reported by different groups.[2,24,25] It was further improved by Aeinehvand *et al.* by replacing a rigid chamber with a latex micro-balloon to decrease the operation spin speed and increase the pumping volume.[17,26,27]

In this paper, we report a novel utilization of elastic membranes covering fluidic chambers to implement inward pumping. The unique feature of the presented design is a combination of the elastic membrane (that provides projection of the fluid toward the disk's center) with a fluidic conduit of two different fluidic resistances. When the fluid is propelled inward, it travels preferentially in the channel of low fluidic resistance, but the fluidic network is designed in a way that the fluid returns downward in the channel of higher fluidic resistance. Therefore, the presented mechanism allows for effective recirculation of the fluid and mixing of fluids in the fluidic network consisting of the upper and lower reservoirs connected by the channels of higher and lower fluidic resistance. In the performed experiments, we demonstrate the efficient mixing of the fluids via recirculation. We evaluate the efficiency of pumping the liquid back to a chamber at the original radial position to be as high as 78%–89%, depending on the initial volume of the liquid. A design that combines the inward pumping and blood/plasma separation was also evaluated as a potential application for the described fluid rerouting mechanism.

II. WORKING PRINCIPLE

Schematic drawings of the inward self-pumping mechanism enabled by an elastic membrane cover and the relevant sequence of fluidic steps are shown in Fig. 1. The CD design in Fig. 1(a) consists of seven components: inlet hole, loading chamber, inlet channel with high fluidic resistance, recirculating chamber with elastic membrane cover, recirculating channel with low fluidic resistance, ventilation hole, and collection chamber. The working principle of the mechanism is shown in Fig. 1(b). Step 1: the liquid is introduced to the loading chamber through the inlet hole. Step 2: the CD spins at high rpm to propel the liquid into the recirculating chamber and inflate the elastic membrane. Step 3: upon fast deceleration, the return of the elastic membrane to its initial position pushes the liquid from the recirculating chamber toward the center of the CD through the two channels that have distinct resistances—a wider channel has lower fluidic resistance than the narrower winding channel of higher fluidic resistance. As the volumetric flow rate of liquid is much higher in the channel with lower resistance (recirculating channel), most of the liquid is pumped inward through the recirculating channel and arrives at the collection chamber, as seen in step 4. The liquid left in the loading chamber and recirculating chamber can be further pumped inward by repeating cycles from step 2 to step 4, denoted as the recirculating cycles.

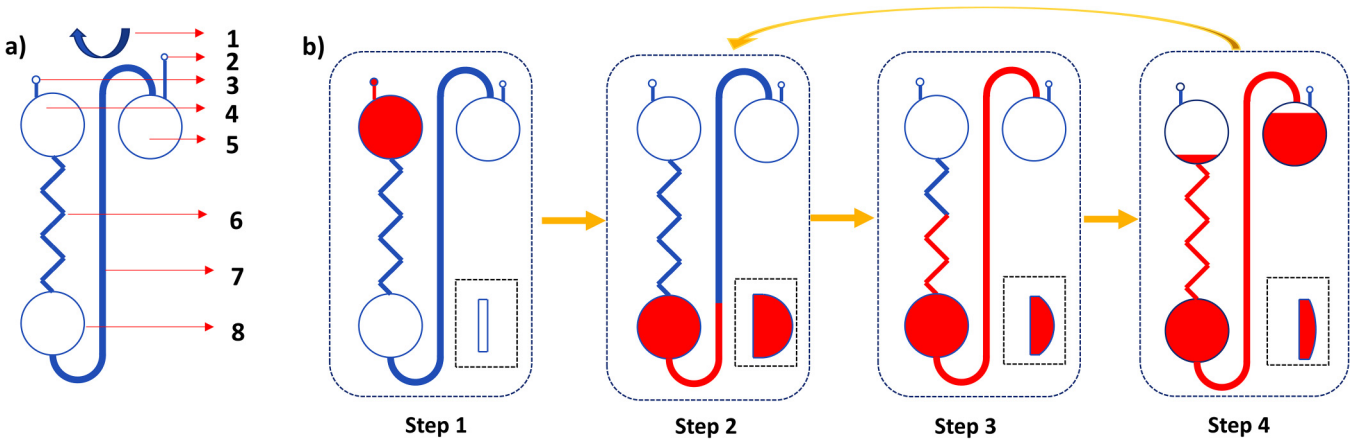

FIG. 1. Schematic drawing of the inward pumping mechanism. (a) The layout of the inward pumping design: 1, The center of rotation; 2, ventilation hole; 3, inlet hole; 4, loading chamber; 5, collection chamber; 6, inlet channel with high fluidic resistance; 7, recirculating channel with low fluidic resistance; 8, recirculating chamber with an elastic membrane cover. (b) The working principle of inward pumping. The dashed boxes show the side view of the recirculating chamber at each step (not to scale). Step 1: sample liquid is injected into the loading chamber through an injection hole. Step 2: the CD is spun at high speed. The liquid in the loading chamber flows through the inlet channel to fill the recirculating chamber and inflate the elastic membrane. Step 3: the angular velocity of the CD decreases rapidly to release the energy that was stored in the membrane. As the elastic membrane returns to its original position, the liquid is pumped inward through both the inlet and recirculating channels. Step 4: since fluid in recirculating channel flows faster than in the inlet channel, most of the liquid is pumped inward through this channel to the collection chamber. After step 4, recirculating cycles steps 2–4 can be conducted to achieve higher inward pumping efficiency.

III. MATERIALS AND METHODS

A. CD design and fabrication

To investigate the elastic membrane-enabled inward pumping mechanism, various CD designs were fabricated and tested. CDs with a radius of 40 mm were designed in SolidWorks (Dassault Systèmes SOLIDWORKS Corp.) and assembled as shown in Fig. 2. The top and bottom CD were machined from PMMA sheets (McMaster-Carr, Elmhurst, IL, USA) with a CNC mill (PCNC 440, Tormach Inc., Waunakee, WI, USA) utilizing the G-code generated by SolidCAM (SolidCAM Ltd., USA). For elastic membrane covers, natural rubber (latex) and PDMS were previously reported as pneumatic components.[17,26,28] In this study, silicone rubber (McMaster-Carr, Elmhurst, IL, USA) and natural rubber (McMaster-Carr, Elmhurst, IL, USA) were selected as the elastic membrane, as elaborated in the supplementary material. Double-sided pressure-sensitive adhesives (FLEXmount® DFM 200 Clear V-95 150 Poly H-9 V-95 400 Poly H-95 4, FLEXcon, MA, USA) were cut into desired circular shapes for the ring adhesive layer and intermediate bonding adhesive layer with a cutter plotter (Silhouette Cameo 4, Silhouette America, Inc., Lindon, UT, USA). The cutter plotter was also used to cut the bottom adhesive layer with single-sided pressure-sensitive adhesive (3M™ 9795R, 3M, Saint Paul, MN, USA). After machining, the CDs were cleaned with DI water and isopropyl alcohol (Sigma Aldrich, St. Louis, MO, USA). The ring adhesives were placed on the shallow terrace at the top CD to bond with the elastic membrane cover. The intermediate bonding adhesive layer was then applied between the top and bottom CD, with the features on both CDs and adhesive being carefully aligned. The bottom adhesive layer was applied to the bottom CD, covering the channels and chambers. The assembled CD was then subjected to pressing five times with a roller press (Dayton's DC Speed Control Roller, Dayton Electric Mfg Co., IL, USA) to ensure strong bonding. After the pressing, the CD was placed under ambient temperature for 24 h before testing.

B. CD testing platform

A centrifugal microfluidic spin stand that we previously reported was used to conduct and observe the experiments (see Fig. S1 in the supplementary material).[29] A brushless DC motor (Anaheim Automation Inc., Anaheim, CA, USA) was controlled by a brushless DC controller (EZSV23, AllMotion, Union City, CA, USA) to spin the CDs. To observe the microfluidic flow on the CDs, a piece of 5 mm wide reflective aluminum adhesive tape (Sigma Aldrich, St. Louis, MO, USA) was placed at the edge of the CD. An IR sensor (PBT46U, Banner Engineering Corp., Minneapolis, MN, USA) sending and receiving an IR beam was placed beneath the edge of the CD as the trigger for the camera's shutter, thus triggering one snapshot of the disk per revolution. A camera (aca800-510uc, Basler, Inc., Exton, PA, USA) and a stroboscope (DT-311A, Shimpo Instrument, Cedarhurst, NY, USA) were used to take pictures when they received the signal from the sensor. Image processing software ImageJ was used to analyze the images.

C. Inward pumping efficiency test

The schematic drawing of the so-called "quantification design" (qCD) is shown in Fig. 3(a). This design is intended to pump liquid inward from a radial distance of 34 mm to a radial distance of 14 mm from the center. The pumping efficiency η is

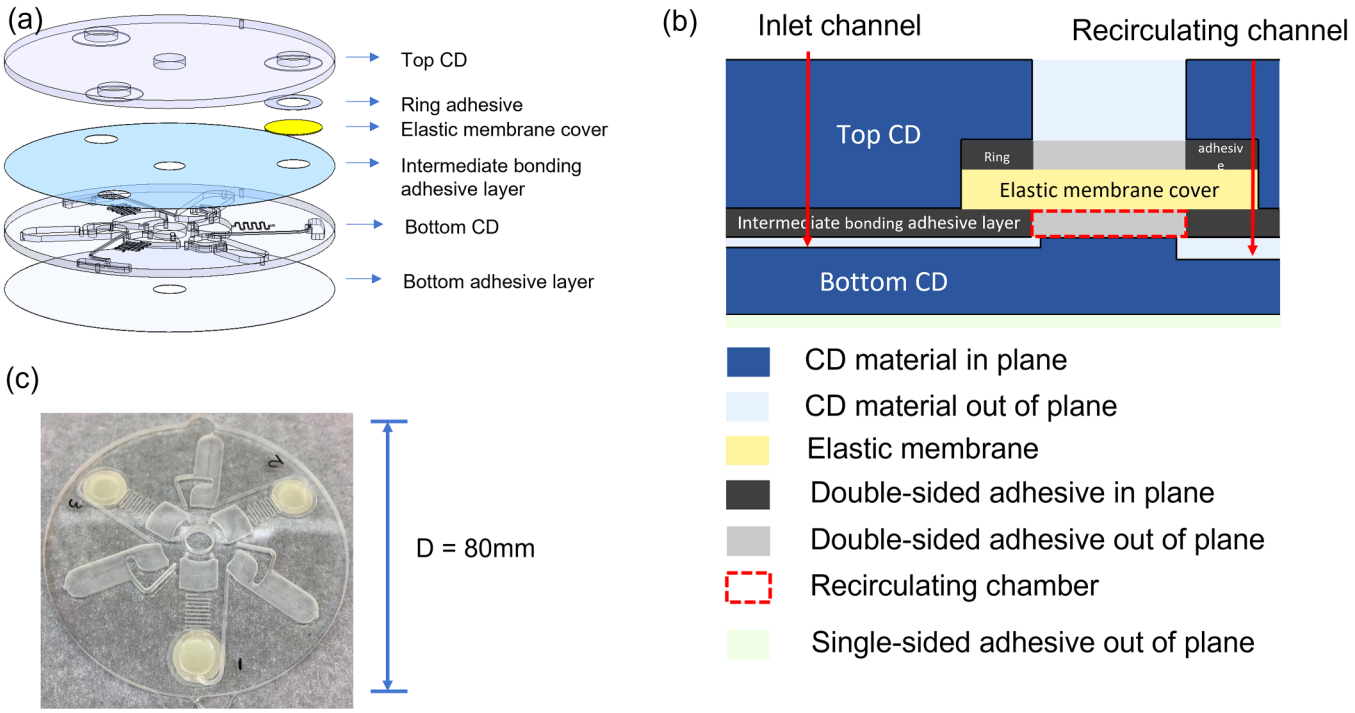

FIG. 2. (a) Detailed layout of the CD components. (b) A schematic cross-sectional view of the recirculation chamber. The red dashed square indicates the recirculation chamber, which has a thickness of 100 μm. (c) A fabricated CD with natural rubber as the elastic membrane.

calculated as

$$\eta = \frac{V_{\text{transferred}}}{V_{\text{initial}}}, \tag{1}$$

where V_{initial} is the volume of fluid initially placed in the loading chamber and $V_{\text{transferred}}$ is the volume of fluid that is pumped into the collection chamber with the leftover volume calculated as

$$V_{\text{leftover}} = V_{\text{initial}} - V_{\text{transferred}}. \tag{2}$$

The collection chamber was designed with a uniform depth so that the transferred volume can be calculated by measuring the area that the liquid covers through processing the images of the chambers taken at the beginning and at the end of the fluid transfer process. To minimize the leftover volume in the recirculating chamber, this chamber was designed to reach a minimum volume when the elastic membrane cover pushes against the bottom CD surface when the CD is stationary. The height of the recirculating chamber corresponds to the thickness of the bonding adhesive, which is 100 μm. After loading the qCD with DI water of various volumes where dye (McMaster-Carr, Elmhurst, IL, USA) was added for the ease of observation, the tests were conducted with a protocol consisting of alternating the spin speed between 3600 and 180 rpm, as shown in Fig. 3(e) and Table S1 in the supplementary material. Once this protocol was finished, the qCD was spun at 1000 rpm again to form a uniform meniscus in the collection chamber. Images of the quantification chambers were taken at this spin speed to calculate the volume of transferred liquid.

D. Recirculation/mixing efficiency test

The recirculation and mixing tests were conducted with a CD design (rmCD) presented in Fig. 3(b). The recirculating channel was designed to guide the liquid back to the loading chamber to complete the recirculation of liquid. To visualize the mixing effect better, a light-colored natural rubber membrane (McMaster-Carr, Elmhurst, IL, USA) was used as the elastic membrane cover for the recirculating chamber. 50 μl of DI water with green dye (McMaster-Carr, Elmhurst, IL, USA) was first injected in the loading chamber through the inlet hole. The CD was spun at 2000 rpm to propel the liquid down to the recirculating chamber. The rmCD was then slowly stopped so that the liquid did not travel through the recirculating channel. 50 μl of DI water with blue dye (McMaster-Carr, Elmhurst, IL, USA) was slowly loaded in the loading chamber through the inlet hole without disturbing the previously loaded liquid. The rmCD was then tested on the spin stand with the same protocol as the inward pumping efficiency test [the spin profile is presented in Fig. 3(e)].

E. Blood/plasma separation and transfer test

The CD design of blood/plasma separation CD (bpsCD) is shown in Fig. 3(c). While similar in design to the qCD, the bpsCD

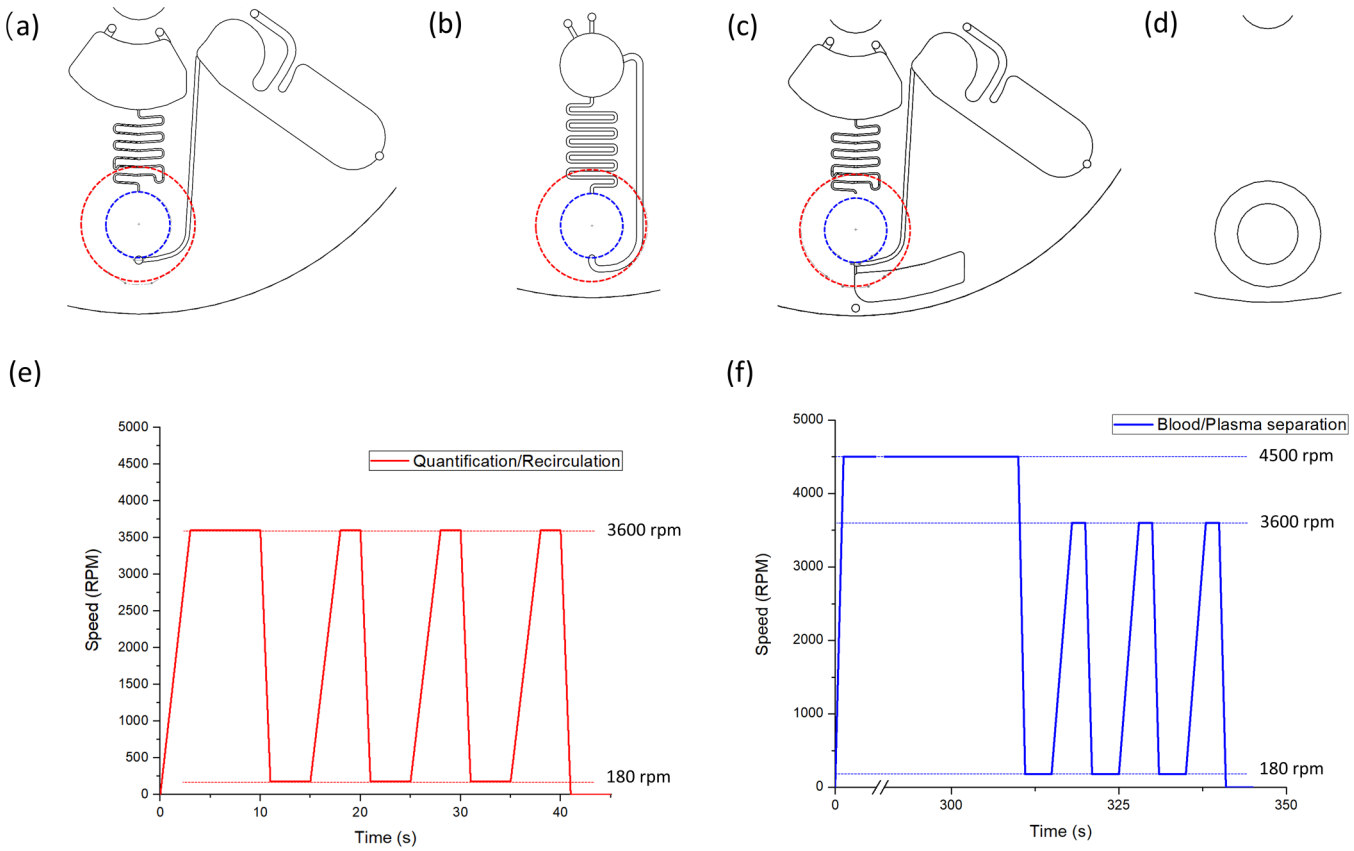

FIG. 3. (a)–(c) Various CD designs. The blue dashed circles indicate the position of the recirculation chamber, and red dashed circles indicate the position of the terrace on the top CD. (a) CD design of quantification CD (qCD). The recirculating channel guides the liquid to a collection chamber. (b) CD design for recirculation/mixing CD (rmCD). The recirculating channel guides the liquid back to the loading chamber. (c) CD design for blood/plasma separation CD (bpsCD). A chamber connecting to the bottom chamber with a small channel was designed to collect the blood cells. (d) Design of the top plastic layer for all CD designs that contain a terrace to place the ring adhesive and elastic membrane. A trough hole leaves enough space for the inflation of the elastic membrane cover. (e) Protocol for quantification test and recirculation/mixing test. The detailed protocol is provided in Table S1 in the supplementary material. (f) Protocol for blood/plasma separation test. The CD is spun at 4500 rpm to perform blood/plasma separation. The detailed protocol is provided in Table S2 in the supplementary material.

has a blood cell chamber with a volume of 75 μl that connects to the bottom of the recirculating chamber. 150 μl of bovine blood (Sigma Aldrich, St. Louis, MO, USA) was injected into the loading chamber through the inlet hole. Blood/plasma separation and transfer tests were conducted using the spin protocol shown in Fig. 3(f), where during the plasma separation step, the bpsCD is spun at 4500 rpm for 5 min. After the test, the bpsCD was spun at 1000 rpm to take quantification images.

IV. RESULTS AND DISCUSSION

A. Inward pumping efficiency

Experiments were conducted to evaluate the inward pumping efficiencies with various initial volumes. To calibrate the camera and image processing software, 80, 100, 120, 140, and 160 μl of the colored DI water were separately loaded into the quantification chamber directly from the ventilation hole. Images were taken with the qCD spinning at 1000 rpm to generate a calibration line (as shown in Fig. S2 in the supplementary material). The inward pumping efficiency tests were conducted with various initial volumes: 100, 120, 140, and 160 μl. The plots of the corresponding transferred volumes of the fluid, the inward pumping efficiency values, and the leftover volumes are presented in Fig. 4.

As shown in Fig. 4(b), with the current design and protocol, the inward pumping efficiency increased from 78% to 89% as the initial volume increased from 100 to 160 μl. Meanwhile, the leftover volume shown in Fig. 4(c) remained approximately the same. To further investigate the influence of the size of the elastic membrane on pumping efficiency, recirculating chambers with different sizes were designed [see Figs. 5(a)–5(c)]. The inward pumping efficiencies and leftover volumes for each design are presented in Figs. 5(d) and 5(e). An overall trend can be observed that, as the initial volume increases, the inward pumping efficiency increases, which agrees with the result shown in Fig. 4(b). Another trend revealed

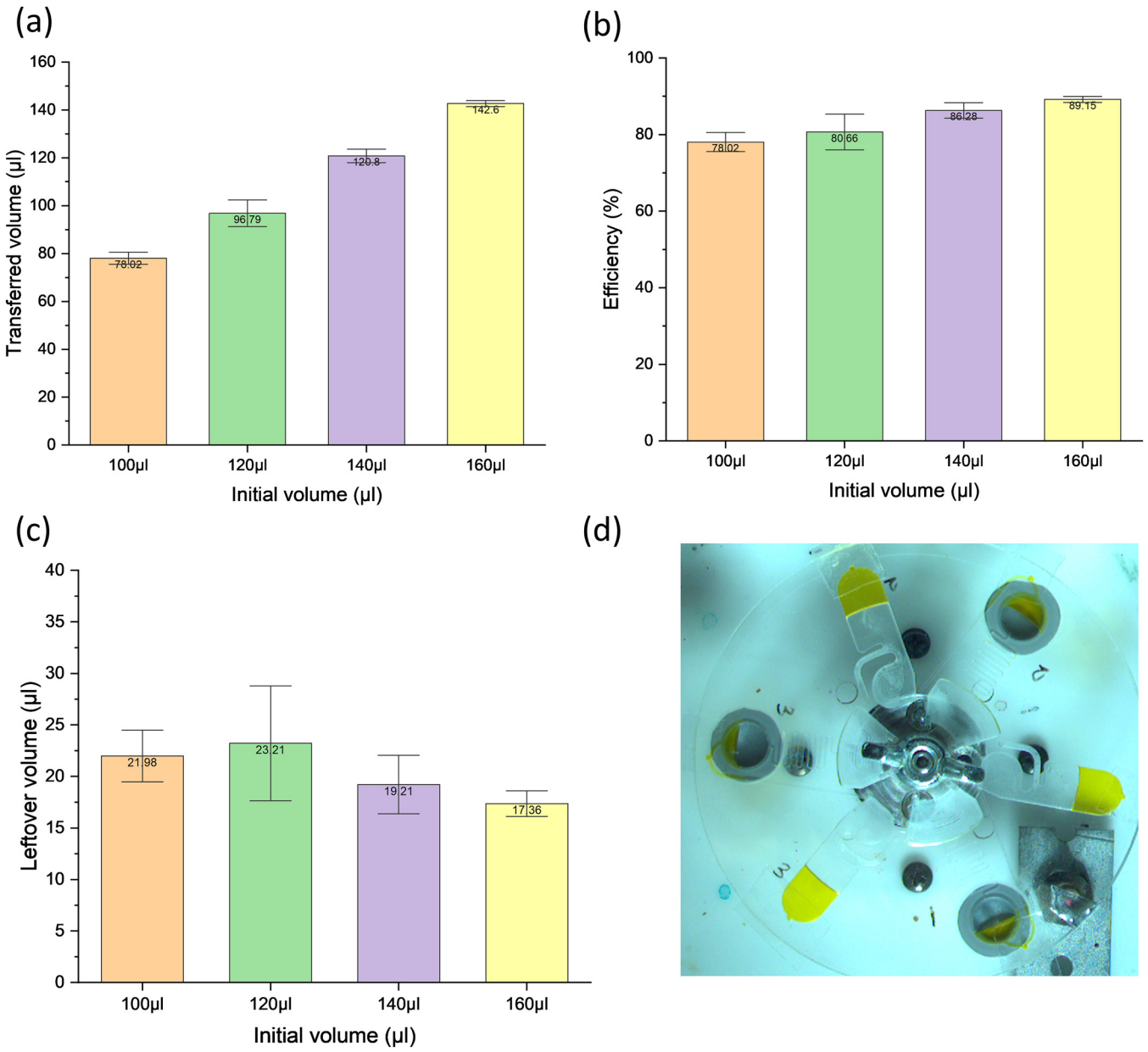

FIG. 4. The inward pumping efficiency tests were conducted with colored DI water. Transferred volumes (a), inward pumping efficiencies (b), and leftover volumes (c) are presented on the respective plots. As the initial volume gets larger, the transfer efficiency gets higher. On the other hand, the leftover volume does not change much as the initial volume varies. A representative image (d) demonstrates the liquid transfer at 1000 rpm. The error bars shown in the graph represent one standard deviation.

by these experiments is that the leftover volume grows with the size of the recirculating chamber. At the same time, the leftover volume remained approximately the same for the same chamber size, despite different initial volumes.

To analyze the process of elastic membrane-enabled inward pumping, screenshots at crucial time points during an inward pumping efficiency test with 140 μl as initial volume are presented in Fig. 6. First, the liquid is loaded into the loading chamber, as shown in Fig. 6(a). Then, the qCD is spun at 3600 rpm, and the liquid transfers to the recirculating chamber, as shown in Fig. 6(b). After fast deceleration to 180 rpm, the liquid travels inward through both the inlet and recirculating channels, as shown in Fig. 6(c). The liquid filled the entire recirculating chamber and not only entered the collection chamber through the recirculation

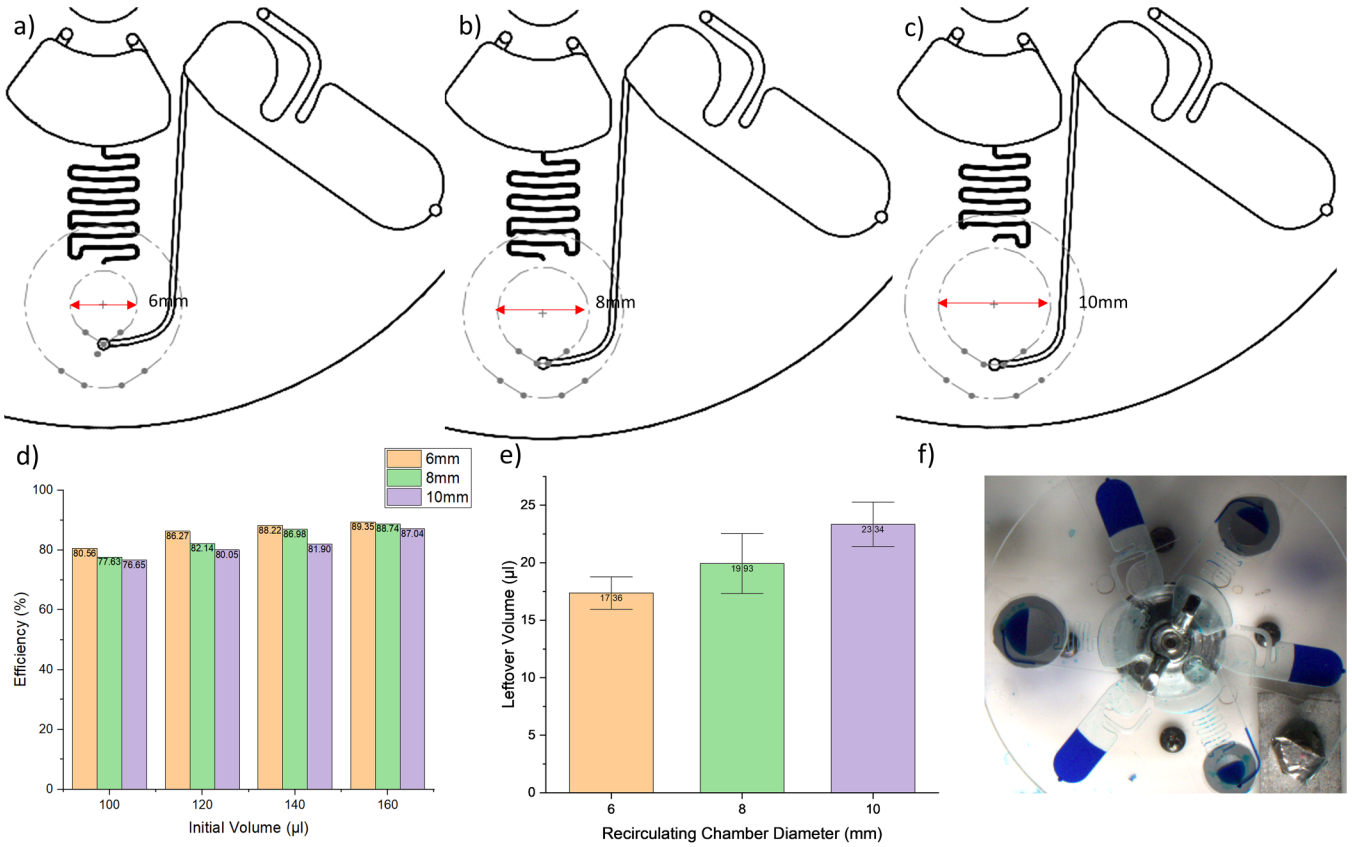

FIG. 5. Inward pumping efficiency designs for CD designs with different diameters of recirculating chambers: (a) 6, (b) 8, and (c) 10 mm. The inward pumping efficiency and the leftover volume for each design are shown in (d) and (e). As the recirculating chamber becomes bigger, the inward pumping efficiency decreases and the leftover volume increases. A representative screenshot of the tests is shown in the inset (f). The error bars on the graph (e) correspond to one standard deviation.

channel but also entered the loading chamber through the inlet channel [indicated by a red circle in Fig. 6(c)]. Then, the qCD was spun at 3600 rpm again to push the fluid into the recirculating chamber, stretching the elastic membrane cover. Since the volume left to be transferred was smaller than the initial volume, the liquid level in the recirculating chamber in Fig. 6(d) was lower than the liquid level in Fig. 6(b). The smaller liquid volume further led to an insufficient liquid filling of the entire recirculating chamber, thus decreasing the amount of stretch of the elastic membrane. Observation found that no liquid was able to flow to the loading chamber at 180 rpm, as shown in Fig. 6(e). In the meantime, there are some remaining liquid drops in the inlet channel that were not transferred to either the loading chamber or the recirculating chamber during the deceleration step. When a steady state was reached, a small meniscus appeared at the entrance of the collection chamber [inside the red circle in Fig. 6(e)], providing surface tension to balance against the compression from the elastic membrane and the centrifugal force from the spinning of the CD. It indicates that the deformation of the elastic membrane in Fig. 6(d) is significant enough to push liquid into the collection chamber. At the end of the third 3600–180 rpm cycle, the meniscus shown in the red circle from Fig. 6(g) is smaller than the meniscus in Fig. 6(e), indicating that the energy stored from the previous step shown in Fig. 6(f) was not enough to pump any liquid further into the collection chamber. Thus, the inward pumping of liquid was completed.

Generally, the starting condition of a recirculating cycle can be categorized into two cases, depending on the volume of liquid left to be transferred. The first case is that with an initial liquid, V_{I1}, the elastic membrane stores enough energy during step 2, which can push the liquid to fill the recirculating chamber and flow back through the inlet channel when the CD decelerates during steps 3 and 4. But, as the resistance of the inlet channel is significantly larger than the resistance of the recirculating channel, most of the liquid will be transferred through the recirculating channel, as denoted with V_{T1}. The volume left to be transferred, which is $V_{I1} - V_{T1}$, will be the initial volume V_{I2} of the next cycle. As the cycles continue, the liquid leftover volume gets smaller. Eventually, the initial volume of a cycle will not be enough to fill the entire recirculating chamber during the deceleration step, which can be

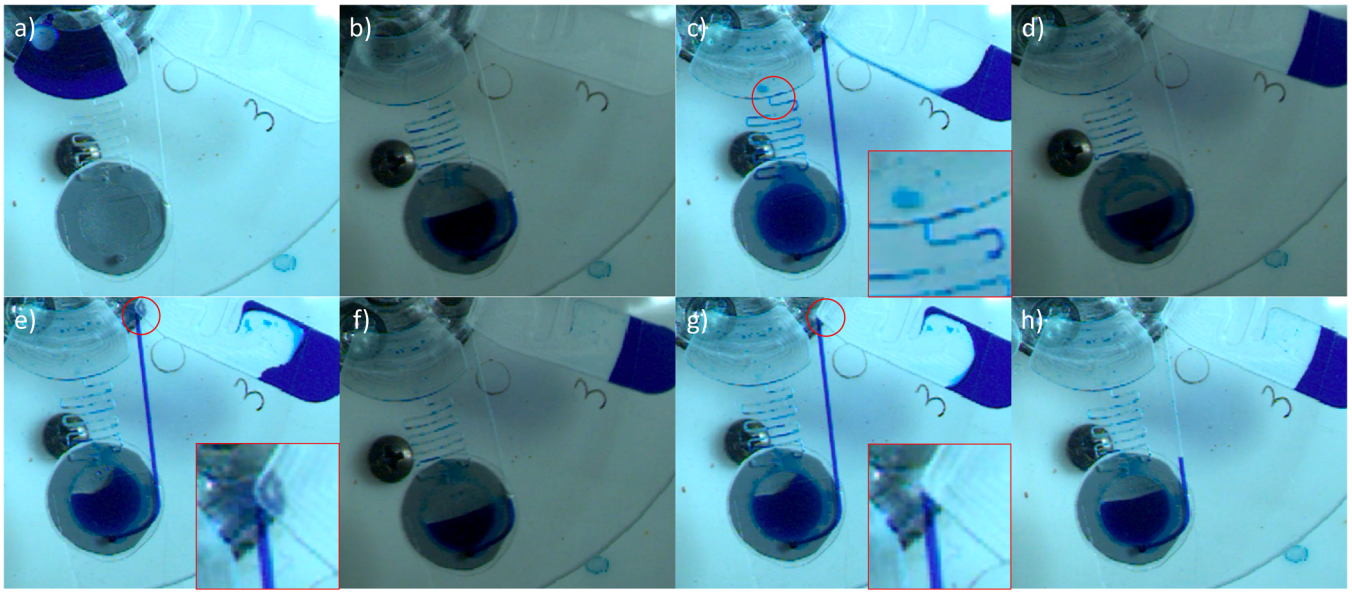

FIG. 6. Screenshots of inward pumping efficiency test with 140 μl of colored DI water. (a) Loading of liquid into the loading chamber. (b) During the high-speed step at 3600 rpm, liquid was transferred from the loading chamber into the recirculating chamber. (c) When the angular velocity was slowed to 180 rpm, liquid entered the loading chamber through the inlet channel as indicated by the red circle. The inset presents the magnified view of the circled region of the image. (d) During the second high-speed step at 3600 rpm, less liquid was stored in the recirculating chamber to inflate the elastic membrane. (e) When the disk's rotation was slowed to 180 rpm again, there was not enough of the liquid to fill the recirculating chamber completely. A meniscus appeared at the boundary of the recirculating channel and collection chamber, indicating the energy was still enough to pump liquid inward. The inset presents the magnified details of the meniscus leading into the collection chamber. (f) During the third high-speed step at 3600 rpm, followed by (g) the third low-speed step at 180 rpm, no more liquid could be transferred into the collection chamber. The inset presented a magnified view of the recirculation channel joining the collection chamber, indicating no further fluid transfer is taking place. (h) After the completion of the fluid transfer tests, the qCD was spun at 1000 rpm to take quantification images.

categorized as the second case. In this case, the deformation of the elastic membrane is not large enough to push liquid columns in trenches and bends of the inlet channel to move inward. These liquid columns, which are called liquid plug valves by other researchers, create a high hydraulic resistance that blocks the channel and prevents any backflow of liquid.[30] Therefore, the energy stored in the elastic membrane can only transfer liquid through the recirculating channel. A final equilibrium stage is reached when a balance is achieved among the pressure generated by the elastic membrane, the pressure head generated by the centrifugal forces on the disk, and the pressure caused by the capillary force.

We conducted a conservative analysis of the equilibrium at the slow-speed (180 rpm) step of the final cycle. To estimate the range of possible leftover volumes, we made several assumptions to simplify the calculation. First, the inlet channel was considered blocked by the liquid plug valves per the previous discussion. Then, to estimate the largest leftover volume, the recirculating chamber was assumed to be filled with liquid at the equilibrium stage. Another assumption was that the shape of the elastic membrane is spherical, which is close to reality when the CD was spun at a low speed, such as 180 rpm. The liquid volume in the inlet channel was neglected in this calculation, as its total volume is 2.98 μl and most of it is occupied by air. Therefore, the pressure generated by the deformation of the elastic membrane, P_m, in terms of the bulge height, h, can be calculated as follows:[26,31,32]

$$P_m(h) = C_1 \frac{Mth^3}{a^4} + C_2 \frac{\sigma_0 th}{a^2}, \tag{3}$$

where t is the thickness of the membrane. a is the radius of the recirculating chamber. C_1 and C_2 are geometrical constants. M is the biaxial modulus of the elasticity of the membrane, which can be calculated using Young's modulus of elasticity E and Poisson's ratio ν,

$$M = \frac{E}{1-\nu}. \tag{4}$$

The pressure balance at equilibrium can be described as

$$P_m = P_c + P_{cap}, \tag{5}$$

where P_c is the centrifugal pressure generated by the liquid column equal to (for the filled recirculating chamber)

$$P_c = \frac{1}{2}\rho\omega^2\left[(r_2 - a)^2 - r_1^2)\right], \tag{6}$$

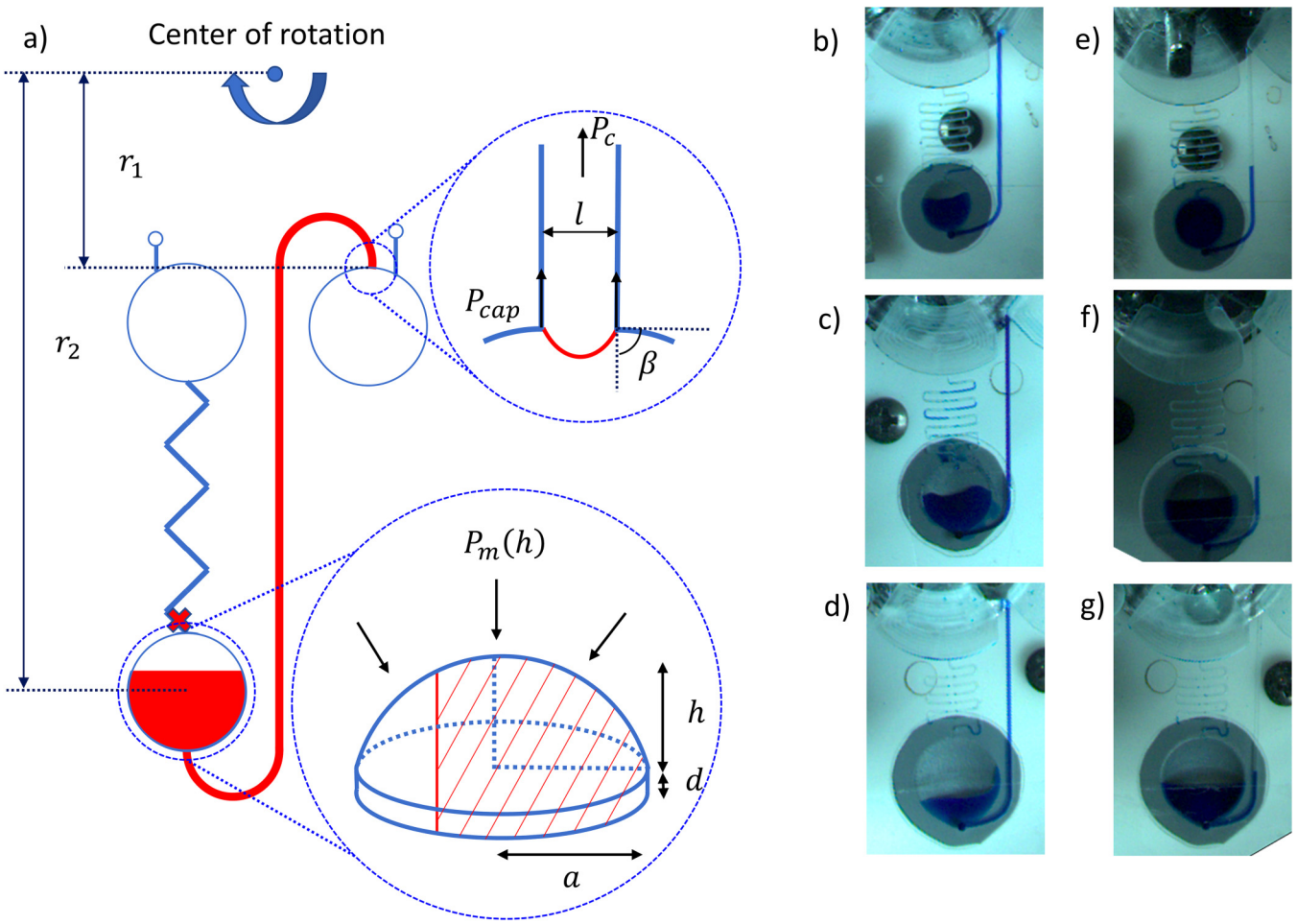

FIG. 7. (a) Schematic drawing related to the analysis of the liquid/membrane equilibrium of the spinning disk. In most cases, the recirculating chamber is partially filled as indicated by the shaded area. To simplify the calculation, we only discuss three situations: fully-filled, half-filled, and empty recirculation chamber. Here, r_1 is the radial position of the exit of the recirculating channel, r_2 is the radial position of the center of the recirculating chamber, θ is the contact angle of water/PMMA, l is the width and height of the recirculating channel with a square cross-sectional area, a is the radius of the recirculating chamber, h is the bulge height of the elastic membrane. The inlet channel was considered blocked and the recirculating chamber was considered filled with liquid. (b)–(d) are screenshots of the recirculating chamber with different radius at 180 rpm after the tests. The filling level of the recirculating chamber gets lower as the recirculating chamber gets larger. (e)–(g) are screenshots taken at the 3600 rpm period of the test. The volume of air trapped in the recirculating chamber gets larger as the chamber size is increased.

while P_{cap} is the capillary pressure that can be described as follows:[33,34]

$$P_{cap} = -\frac{3\sigma\cos\theta_p^* + \sigma\cos\theta_a}{4l}, \tag{7}$$

where ρ is the density of the liquid, ω is the angular speed of the CD, r_1 is the radial position of the exit of the recirculating channel, r_2 is the radial position of the center of the recirculating chamber, σ is the surface energy of the water/air interface, θ_p^* is the contact angle at the exit of the recirculating channel, described by $\theta_p^* = \min\{\theta_p + \beta, 180^\circ\}$,[33] θ_p is the contact angle of water/PMMA, β is the angle change at the exit of the recirculating channel, θ_a is the contact angle of water/adhesive,[34] and l is the width and height of the recirculating channel with a square cross-sectional area. A schematic drawing relating to the outlined analysis is presented in Fig. 7(a).

By substituting Eqs. (3), (4), (6), and (7) into Eq. (5), we obtain Eq. (8)

$$C_1\frac{Eth^3}{(1-\nu)a^4} + C_2\frac{\sigma_0 th}{a^2} = \frac{1}{2}\rho\omega^2\left[((r_2-a)^2 - r_1^2)\right] - \frac{3\sigma\cos\theta_p^* + \sigma\cos\theta_a}{4l}. \tag{8}$$

TABLE I. Parameters used for volume calculation.

Parameters	Value	Parameters	Value
C_1	8/3	θ_p	68°
C_2	2	σ	40 mJ/m^2
r_1	11.5 mm	l	0.5 mm
r_2	29 mm	ρ	10^3 kg/m^3
a	3, 4, and 5 mm	ω	6π/s
d	100 μm	t	100 μm
θ_a	110.5°	β	90°
σ_0	0 MPa	L when $a = 3$	34.04 mm
E	0.135 MPa	L when $a = 4$	34.88 mm
ν	0.48	L when $a = 5$	35.84 mm

As the elastic membrane was assembled with no initial stress, the value of σ_0 is 0. The equation can be simplified as follows:

$$C_1\frac{Mth^3}{a^4} = \frac{1}{2}\rho\omega^2\left[((r_2-a)^2 - r_1^2)\right] - \frac{3\sigma\cos\theta_p^* + \sigma\cos\theta_a}{4l}. \quad (9)$$

To calculate the volume of the recirculating chamber, the bulge height was calculated

$$h = \sqrt[3]{a^4(1-\nu)\times\frac{\frac{1}{2}\rho\omega^2\left[((r_2-a)^2 - r_1^2)\right] - \frac{3\sigma\cos\theta_p^* + \sigma\cos\theta_a}{4l}}{C_1Et}}. \quad (10)$$

The volume of the recirculating chamber can be calculated using a hemispherical cap approximation

$$V_{Re} = \frac{2}{3}\pi a^2 h. \quad (11)$$

Therefore, the maximum leftover volume $V_{leftmax}$ can be calculated from the following equation:

$$V_{leftmax} = \frac{2}{3}\pi a^2 h + Ll^2 + \pi a^2 d, \quad (12)$$

where L is the length of the recirculating channel and l is the width and height of the recirculating channel, d is the thickness of the bonding adhesive. The parameters used for the calculation are listed in Table I.

We also calculated the volumes when the recirculating chamber is half-filled with liquid or empty. The equations for each situation are

Half-filled,

$$h = \sqrt[3]{a^4(1-\nu)\times\frac{\frac{1}{2}\rho\omega^2(r_2^2 - r_1^2) - \frac{3\sigma\cos\theta_p^* + \sigma\cos\theta_a}{4l}}{C_1Et}}, \quad (13)$$

$$V_{leftmax} = \frac{1}{3}\pi a^2 h + \frac{1}{2}\pi a^2 d + Ll^2. \quad (14)$$

Empty,

$$h = \sqrt[3]{a^4(1-\nu)\times\frac{\frac{1}{2}\rho\omega^2\left[((r_2+a)^2 - r_1^2)\right] - \frac{3\sigma\cos\theta_p^* + \sigma\cos\theta_a}{4l}}{C_1Et}}, \quad (15)$$

$$V_{leftmax} = Ll^2. \quad (16)$$

To compare the calculated result with the experimental result, the filling ratios of the recirculating chamber for average experimental results, η, were introduced here, which can be calculated by the following equation:

$$\eta = \frac{V_{leftexp} - Ll^2}{\frac{2}{3}\pi a^2 h + \pi a^2 d}, \quad (17)$$

where $V_{leftexp}$ is the average experimental leftover volume. The calculated volumes and the average experimental volumes are shown in Table II. The volumes for fully filled chambers and the volumes for empty chambers set the range of the possible leftover volume. As the chamber radius increases, the higher and lower limits of the possible leftover volume get larger. Meanwhile, the window for possible leftover volume gets bigger, which agrees with the trend in the experimental data. However, the filling ratio of the recirculating chamber gets smaller when the chamber size is increased, which has also been observed in experiments as shown in Figs. 7(b)–7(d). The latter can be explained by the fact that during the high-rpm

TABLE II. Calculated leftover volumes with different radii and different filling conditions corresponding to different tested volumes. The tested volumes sit between the volume for fully filled chambers and the volume for empty chambers.

Radii of the recirculating chamber (mm)	Volumes for fully filled chamber (μl)	Volumes for half-filled chamber (μl)	Volumes for empty chamber (μl)	Average experimental volumes (μl)	Filling ratio of the recirculating chamber (%)
3	22.10	15.62	8.51	17.36	65.11
4	41.29	26.09	8.72	19.93	34.42
5	73.62	44.15	8.96	23.34	22.24

spin, the volume of the air trapped in the recirculating chamber becomes larger as the radius of the recirculating chamber gets bigger. The increase in trapped air volume contributes to a reduction in the filling ratio of the recirculating chamber as the chamber radius increases.

In general, to obtain a higher inward pumping efficiency for a specific amount of initial volume, a smaller chamber is desired as it has a smaller leftover volume. As a trade-off, the smaller chamber holds a smaller amount of liquid, leading to a limited amount of liquid pumped for each cycle. Therefore, a smaller chamber requires more cycles to complete the inward pumping when a large initial volume is loaded. Another concern for the small recirculating chamber is that with a large initial volume, the pressure generated during high speed can cause the deterioration of the elastic membrane and delamination of the adhesives. Therefore, the chamber diameter should be designed according to the initial volume and desired inward pumping efficiency.

B. Recirculation/mixing capabilities

In microfluidic systems, reagent rehydration and hybridization of biomolecules often require fluidic systems to have appropriate mixing capabilities to achieve reliable results within a short timeframe.[35] To evaluate the mixing capability of the inward pumping mechanism, experiments were conducted with the design shown in Fig. 3(b) and the spin profile is shown in Fig. 3(e). The working principle of the recirculation/mixing design is shown in Fig. 8.

Screenshots were made, as shown in Figs. 9(a)–9(f). It can be seen from Figs. 9(d) and 9(f) that most of the liquid that was pumped inward traveled through the recirculating channel, as the inlet channel remains partially filled. These screenshots were processed with ImageJ to split into red, green, and blue channels for ease of measurement. Histograms for the blue channel were taken and shown next to the corresponding screenshots to evaluate the mixing efficiency. The center of the disk was selected as the sampling area for ease of assessment. The standard deviations of the pixel intensity in the blue channel were used as mixing indexes to evaluate the mixing efficiency.[36] As shown in the histograms, the standard deviations got smaller as the test went on, reaching a value of 6.439 at the end of the second cycle. As the test continued, the standard deviation remained around 6.5, indicating that mixing was complete.

As the fluidic mixing happened during the fast deceleration step shown in Fig. 9(c), we hypothesize that the mixing was a result of the elongation of the laminar fluidic interface due to the Euler force, which can be described by

$$F_e = \rho r \frac{d\omega}{dt}, \tag{18}$$

where ρ is the density of the fluidic, r is the radial distance, $\frac{d\omega}{dt}$ is the acceleration/deceleration rate of the CD. As the Euler force is linearly dependent on the radial position, the liquid in the recirculating chamber features an Euler force gradient in the radial direction, leading to a vortex forming in the chamber, as shown in Fig. 9(c) and Video S1 in the supplementary material. This vortex folds the layers of fluid together and thus minimizes the diffusion length and greatly enhances mixing and homogenization, which is consistent with other results from the literature and is especially important when operating in the laminar fluidic regime (as seen in the supplementary material).[37] At the same time, the liquid was pumped inward through the recirculating channel without being mixed by the vortex. This portion of liquid could only join the mixing event after the second 3600 rpm step, shown in Fig. 9(e). Therefore, a minimum of two cycles is required to complete the mixing. Besides, this recirculation design created a circular fluidic

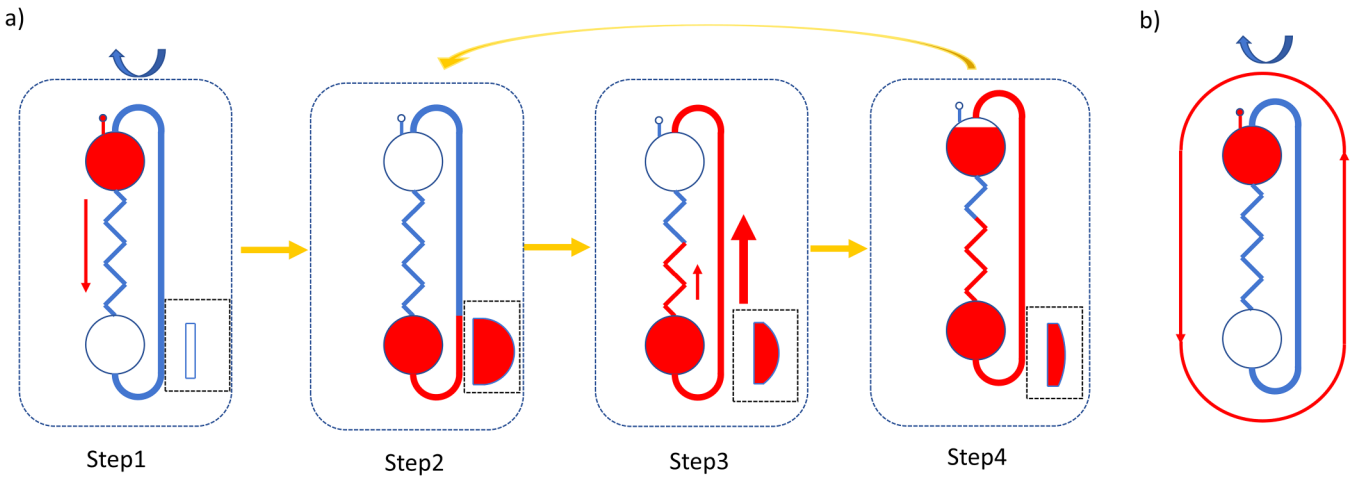

FIG. 8. (a) Schematics of the recirculation/mixing process. Multiple recirculation events can be carried out by repeating cycles from step 2 to step 4. The dashed boxes show the side view of the recirculating chamber at each step (not to scale). (b) The liquid in the recirculation/mixing design flows radially outward through the inlet channel during high speed (3600 rpm) and radially inward through the recirculating channel during low speed (180 rpm), forming a circular fluidic route, which can be beneficial for mixing.

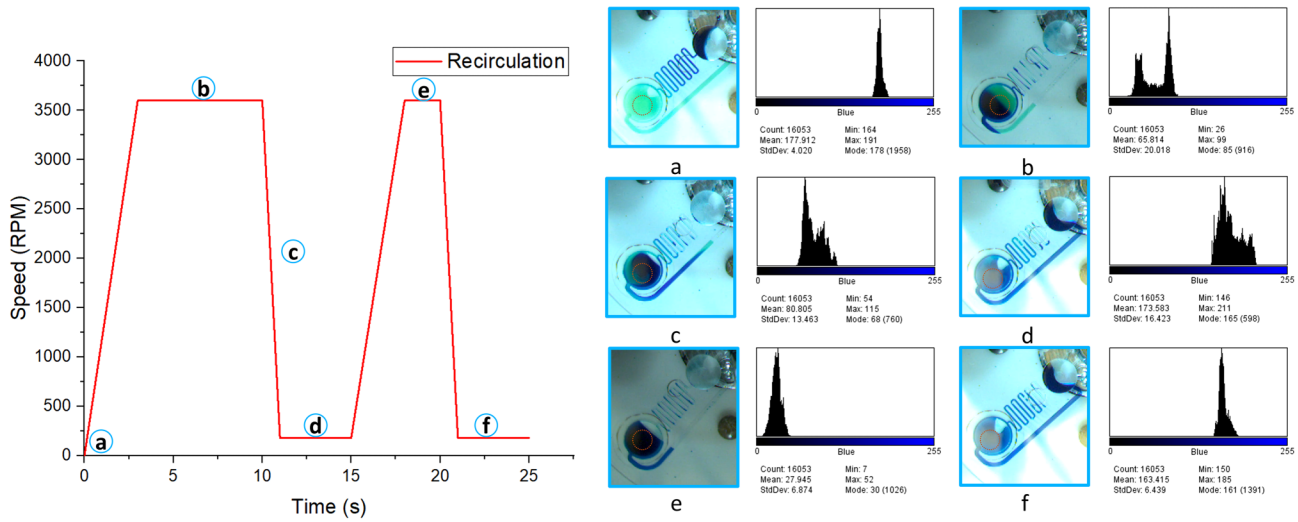

FIG. 9. The recirculation and mixing efficiency test. As shown in the screenshots (a)–(f), the liquid was moved in a circular pattern, with no liquid returning to the loading chamber through the inlet channels. The histograms of the color intensity inside the circled area in the recirculating chamber are shown next to the corresponding screenshots, indicating the mixing was completed during the second cycle.

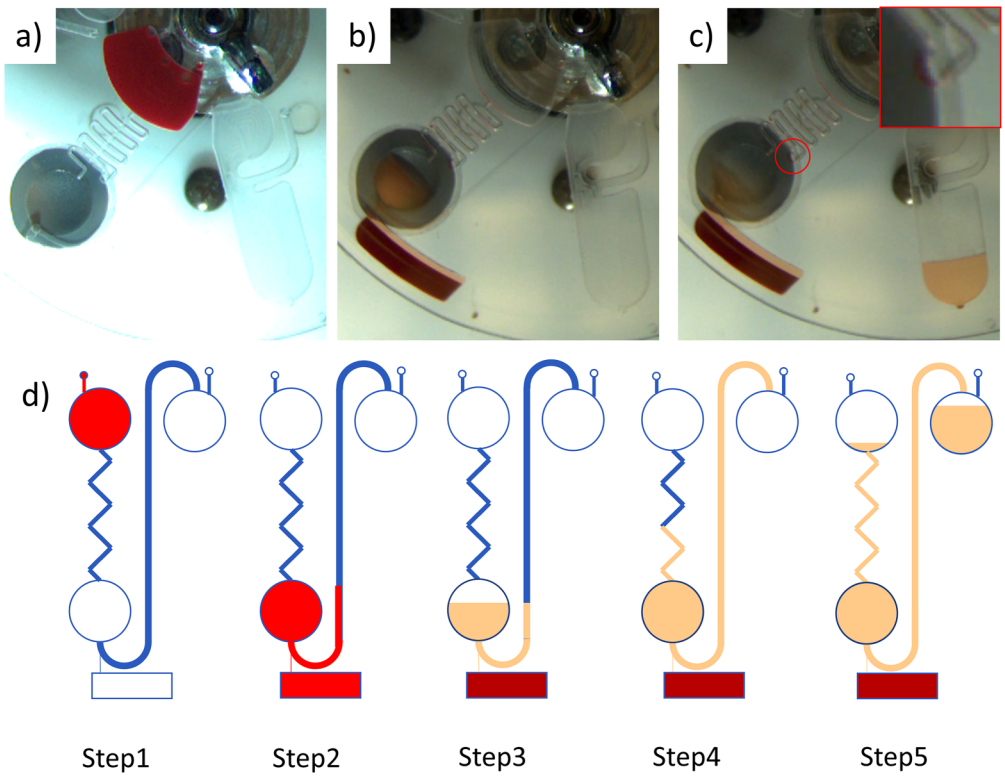

FIG. 10. Blood/plasma separation and inward pumping were achieved using the bpsCD. (a) Loading 150 μl bovine blood into the loading chamber. (b) Blood/plasma separation at 4500 rpm. (c) Through multiple cycles, the plasma was transferred to the collection chamber. The red circle indicates the region where the red blood cells sediment in the channel. The inset is the enlarged picture of the red circle for clarity. (d) A schematic drawing of the blood/plasma separation test.

route that allowed the liquid to flow in one way in the channels (radially inward through the recirculating channel and radially outward through the inlet channel), ensuring a faster mixing. It is essential for reagent rehydration, where the liquid with a longer residence time with the reagent usually has a higher reagent concentration than the liquid with a shorter residence time.[12,35] Another potential application is for accelerating diffusion-limited reactions, where the liquid usually generates a depletion region after it flows through the reaction area.[38] This mechanism reduces the depletion region by mixing the liquid, which has flowed through the reaction region with the liquid that has not, which is still abundant in reactive species.

C. Elastic membrane based blood/plasma fluidic unit integrated on the CD platform

In addition to enhancing reagent rehydration and speeding up diffusion-limited reactions through the mixing and recirculating capabilities, the elastic membrane-based recirculation also enables better utilization of real estate on the CD, by transferring the liquid that reaches the edge of the CD to the center of another sector. For example, one of the most widely used point-of-care testing sample preparation steps is the blood/plasma separation, which is usually the first step of most blood-related biological assays. However, when implemented on a centrifugal microfluidic disk, the features need to be located at the edge of the CD to fully utilize the centrifugal force.[2] Without any inward pumping approaches, the CD has to be larger to accommodate any other steps. As an example application for the mechanism, we designed, fabricated, and tested a bpsCD with 150 μl bovine blood, as shown in Fig. 3(c). A schematic drawing of the test protocol and results are shown in Fig. 10. The design had a small channel connecting the recirculating chamber and the 75 μl blood cell chamber, preventing the backflow of red blood cells during deceleration. After being separated from the blood, the remaining 75 μl of plasma was transferred to the collection chamber through the same cycles as in the inward pumping efficiency tests. The calculated inward pumping efficiency for plasma was 86% higher than for the DI water with an even higher initial volume. This was mainly because during step 2, blood was transferred under high spin speed and started to separate in the trenches and bends of the inlet channel. As shown in the red circle in Fig. 10(c), the blood cells sedimented blocked the inlet channel, further increasing resistance for plasma to flow inward through the inlet channel. As a result, the recirculating channel became the only outlet out of the recirculation chamber. Therefore, the leftover liquid in this test was less than in the quantification test performed with DI water, providing a higher transfer efficiency.

V. CONCLUSIONS AND OUTLOOK

In this work, we demonstrated a novel inward pumping mechanism for the centrifugal microfluidic platform that requires no external equipment. This mechanism uses an elastic membrane to store and release energy. Through multiple cycles, liquid can be guided to the center of the CD through a recirculating channel. Inward pumping efficiency tests were carried out to evaluate the fluid transfer mechanism. An inward pumping efficiency of over 78% was achieved with various initial volumes and recirculating chamber designs. An analysis that used conservative assumptions was conducted to estimate the range of leftover volume for the recirculating chamber with different sizes. Recirculation and mixing tests were also conducted to explore the potential applications of this fluid transfer mechanism, demonstrating its mixing capability and the unique ability to move liquid in a circular fluidic route, as shown in Fig. 8. A design that combined this mechanism with blood/plasma separation was also fabricated and tested with bovine blood, indicating a plasma pumping efficiency of 86%. These results showed a tunable inward pumping mechanism for liquid manipulation on the centrifugal microfluidic platform with high efficiency and unique liquid movement capabilities as a powerful tool in reaction enhancement and assay integration.

Although the use of elastic membranes on CDs would lead to significant advantages, as demonstrated in this study, the manufacturing method described in our manuscript, while working well for producing a limited number of disks, would be too cumbersome for mass production. The thin elastic membrane inserts are difficult to be handled either manually or with pick and place robotic arms. The use of adhesive for bonding further complicates the fabrication process. Such processes can be simplified by using elastic membranes with the size same as the CD (as shown in Fig. S4 in the supplementary material) and replacing the adhesive bonding with ultrasonic welding. Therefore, the elastic membranes can be welded to the plastic layer. Another concern is that the chemical and environmental compatibilities of rubber vary depending on its composition. For example, silicone rubber used in this research is intolerant to acids and alkalines, limiting the application such as chemical cell lysing, which uses an alkaline solution to extract the genomic substance from cells. At the same time, the natural rubber can withstand acids and alkaline solutions, but it degrades under UV exposure, leading to instability of the mechanism and a shorter shelflife. Therefore, there are still obstacles to overcome before implementing this mechanism in μTAS for assays to be performed in POC scenarios. Finally, wear and delamination of elastic membranes under applied stress is a concern for reliable use of the presented inward-pumping mechanism and should be studied further.

SUPPLEMENTARY MATERIAL

See the supplementary material for Figs. S1 and S2, Tables S1 and S2, and Video S1.

ACKNOWLEDGMENTS

This research is financially supported by Autonomous Medical Devices Incorporated.

AUTHOR DECLARATIONS

Conflicts of Interest

The authors have no conflicts to disclose.

DATA AVAILABILITY

The data that support the findings of this study are available from the corresponding author upon reasonable request.

REFERENCES

[1]M. Madou, J. Zoval, G. Jia, H. Kido, J. Kim, and N. Kim, Annu. Rev. Biomed. Eng. **8**, 601 (2006).
[2]R. Gorkin, J. Park, J. Siegrist, M. Amasia, B. S. Lee, J. M. Park, J. Kim, H. Kim, M. Madou, and Y. K. Cho, Lab Chip **10**, 1758 (2010).
[3]M. Tang, G. Wang, S.-K. Kong, and H.-P. Ho, Micromachines **7**, 26 (2016).
[4]M. Amasia, M. Cozzens, and M. J. Madou, Sens. Actuators, B **161**, 1191 (2012).
[5]G. Czilwik, T. Messinger, O. Strohmeier, S. Wadle, F. Von Stetten, N. Paust, G. Roth, R. Zengerle, P. Saarinen, J. Niittymäki, K. McAllister, O. Sheils, J. O'Leary, and D. Mark, Lab Chip **15**, 3749 (2015).
[6]S. J. Oh, B. H. Park, G. Choi, J. H. Seo, J. H. Jung, J. S. Choi, D. H. Kim, and T. S. Seo, Lab Chip **16**, 1917 (2016).
[7]M. Shen, Y. Chen, Y. Zhu, M. Zhao, and Y. Xu, Anal. Chem. **91**, 4814 (2019).
[8]M. Geissler, D. Brassard, L. Clime, A. V. C. Pilar, L. Malic, J. Daoud, V. Barrère, C. Luebbert, B. W. Blais, N. Corneau, and T. Veres, Analyst **145**, 6831 (2020).
[9]S. Soroori, L. Kulinsky, H. Kido, and M. Madou, Microfluid. Nanofluidics **16**, 1117 (2014).
[10]Y. K. Cho, J. G. Lee, J. M. Park, B. S. Lee, Y. Lee, and C. Ko, Lab Chip **7**, 565 (2007).
[11]H. Kido, M. Micic, D. Smith, J. Zoval, J. Norton, and M. Madou, Colloids Surf., B **58**, 44 (2007).
[12]L. Clime, D. Brassard, M. Geissler, and T. Veres, Lab Chip **15**, 2400 (2015).
[13]J. F. Hess, S. Zehnle, P. Juelg, T. Hutzenlaub, R. Zengerle, and N. Paust, Lab Chip **19**, 3745 (2019).
[14]K. Abi-Samra, L. Clime, L. Kong, R. Gorkin, T. H. Kim, Y. K. Cho, and M. Madou, Microfluid. Nanofluidics **11**, 643 (2011).
[15]M. C. R. Kong and E. D. Salin, Anal. Chem. **82**, 8039 (2010).
[16]Z. Cai, J. Xiang, B. Zhang, and W. Wang, Sens. Actuators, B **206**, 22 (2015).
[17]F. O. Romero-Soto, M. M. Aeinehvand, and S. O. Martinez-Chapa, Mater. Today Proc. **48**(Pt. 1), 50–55 (2022).
[18]Z. Noroozi, H. Kido, and M. J. Madou, J. Electrochem. Soc. **158**, P130 (2011).
[19]R. Gorkin, L. Clime, M. Madou, and H. Kido, Microfluid. Nanofluidics **9**, 541 (2010).
[20]J. L. Garcia-Cordero, L. Basabe-Desmonts, J. Ducrée, and A. J. Ricco, Microfluid. Nanofluidics **9**, 695 (2010).
[21]E. Pishbin, M. Eghbal, S. Fakhari, A. Kazemzadeh, and M. Navidbakhsh, Micromachines **7**, 215 (2016).
[22]M. C. R. Kong, A. P. Bouchard, and E. D. Salin, Micromachines **3**, 1 (2012).
[23]S. Soroori, J. M. Rodriguez-Delgado, H. Kido, G. Dieck-Assad, M. Madou, and L. Kulinsky, Microfluid. Nanofluidics **20**, 1 (2016).
[24]S. Zehnle, F. Schwemmer, G. Roth, F. Von Stetten, R. Zengerle, and N. Paust, Lab Chip **12**, 5142 (2012).
[25]N. Godino, R. Gorkin III, A. V. Linares, R. Burger, and J. Ducrée, Lab Chip **13**, 685 (2013).
[26]M. M. Aeinehvand, F. Ibrahim, S. W. Harun, W. Al-Faqheri, T. H. G. Thio, A. Kazemzadeh, and M. Madou, Lab Chip **14**, 988 (2014).
[27]M. M. Aeinehvand, F. Ibrahim, S. W. Harun, I. Djordjevic, S. Hosseini, H. A. Rothan, R. Yusof, and M. J. Madou, Biosens. Bioelectron. **67**, 424 (2015).
[28]O. C. Jeong and S. Konishi, J. Microelectromech. Syst. **15**, 896 (2006).
[29]J. Siegrist, R. Gorkin, L. Clime, E. Roy, R. Peytavi, H. Kido, M. Bergeron, T. Veres, and M. Madou, Microfluid. Nanofluidics **9**, 55 (2010).
[30]R. Burger, N. Reis, J. G. Da Fonseca, and J. Ducrée, J. Micromech. Microeng. **23**, 035035 (2013).
[31]R. J. Hohlfelder, *Bulge and Blister Testing of Thin Films and Their Interfaces* (Stanford University, 1999).
[32]M. Gad-el-Hak, *MEMS: Design and Fabrication* (CRC Press, 2021).
[33]M. Bauer, M. Ataei, M. Caicedo, K. Jackson, M. Madou, and L. Bousse, Microfluid. Nanofluidics **23**, 1 (2019).
[34]J. Siegrist, M. Amasia, N. Singh, D. Banerjee, and M. Madou, Lab Chip **10**, 876 (2010).
[35]S. Hin, N. Paust, M. Keller, M. Rombach, O. Strohmeier, R. Zengerle, and K. Mitsakakis, Lab Chip **18**, 362 (2018).
[36]Z. Noroozi, H. Kido, M. Micic, H. Pan, C. Bartolome, M. Princevac, J. Zoval, and M. Madou, Rev. Sci. Instrum. **80**, 075102 (2009).
[37]C. Y. Lee, C. L. Chang, Y. N. Wang, and L. M. Fu, Int. J. Mol. Sci. **12**, 3263 (2011).
[38]J. Li, P. Zrazhevskiy, and X. Gao, Small **12**, 1035 (2016).